Applied Clay Science 155 (2018) 57–64

Contents lists available at ScienceDirect

Applied Clay Science

journal homepage: www.elsevier.com/locate/clay

Research paper

Resonance energy transfer between dye molecules in hybrid films of a layered silicate, including the effect of dye concentration thereon

S. Belušáková[a,b], R. Sola-Llano[c], I. Lopez Arbeloa[c], V. Martínez-Martínez[c,*], J. Bujdák[a,b,*]

[a] Comenius University in Bratislava, Department of Physical and Theoretical Chemistry, Faculty of Natural Sciences, 842 15 Bratislava, Slovakia
[b] Institute of Inorganic Chemistry, Slovak Academy of Sciences, 845 36 Bratislava, Slovakia
[c] Molecular Spectroscopy Laboratory, Departamento de Química Física, University of the Basque Country, UPV/EHU, P.O. Box 644, 48080 Bilbao, Spain

ARTICLE INFO

Keywords:
Fluorescence
Fret
Oxazine
Rhodamine
Saponite
Clay

ABSTRACT

Rhodamine 6G (R6G) and Oxazine 4 (Ox4), considered a "Förster Resonance Energy Transfer" (FRET) pair due to the significant overlap between the fluorescence of R6G (as energy donor, ED) and the absorption band of Ox4 (as energy acceptor, EA), were intercalated into an expandable layered silicate, saponite (Sap). Several films with different dyes/Sap loadings were prepared with the aim of studying the energy transfer process between both dyes at variable concentrations in the solids. The films were characterized by spectral methods in the visible spectral range. A theoretical model of FRET efficiency was proposed for hybrid solid materials, built around the construction of probability density functions of the intermolecular distances in the solids. The theoretical results were compared with FRET efficiencies determined experimentally using steady-state and time-resolved fluorescence spectroscopy. Considering the very high sensitivity of the FRET efficiency to the intermolecular distances between ED and EA, the theoretical model could predict experimental data relatively well only for low dye loadings (< 1% of cation exchange capacity). The main reasons for the failure of the model at higher dye loadings were dye aggregation and the occurrence of ED species which did not participate in FRET.

1. Introduction

One of the current aims of modern materials sciences is to design structurally-organized supramolecular systems that are capable of performing useful functions, such as harvesting solar energy and then transferring it for conversion and/or storage (Diacon et al., 2010). One of the most inspiring natural processes is photosynthesis, in which organisms are able to capture light and transfer it efficiently to the reaction center. In that respect, the Förster Resonance Energy Transfer (FRET) process is a very similar photophysical phenomenon. The process starts with the absorption of photons by molecules acting as light harvesting antennas, resulting in electronic excited states. The excited molecules act as energy donors (ED), and fast, non-radiant energy transfer takes place in the presence of energy acceptor molecules (EA). The main requirements for efficient resonance between ED and EA molecules are short intermolecular distances, an appropriate orientation, and spectral overlap between the emission spectrum of ED and the absorption spectrum of EA. There is at present considerable interest in the construction of such materials whose properties arise from interaction between molecules at a nanoscale level, and in improvement of their efficiency. In this context, artificial photonic systems capable of efficient energy transfer have been prepared from chromophores organized in various matrices and systems, such as in zeolites, as a part of metal complexes, polymeric substances, in Langmuir–Blodgett films, inorganic matrices, etc. (Epelde-Elezcano et al., 2016; Sapsford et al., 2004; Zhong, 2009; Zhou et al., 2011). Depending on the structure of these matrices, the energy transfer can be carried out in uni- or bidirectional way, or in two- or three-dimensional space (Calzaferri, 2008; Li et al., 2006). The crucial parameters for FRET in such systems are the organization of dye molecules in the host matrices, and the relative position (both distance and orientation) of the interacting molecules (Zhou et al., 2011). Suppression of undesired dye molecular aggregation to protect the photoactivity of the chromophores is also required.

The simplest systems exhibiting FRET consist of common commercially available dyes embedded in layered silicate hosts. Saponite intercalated with a luminescent polyhedral oligomeric silsesquioxane and rhodamine B has been reported as an example of light-harvesting materials (Olivero et al., 2014). FRET has also occurred between hydrocarbons in organoclays (Neumann et al., 2002), in luminescent polymer/layered silicate nanocomposites (Giovanella et al., 2014), covalently-bound fluorophores on layered silicate (Kuroda et al., 2010; Fujii et al., 2011), and systems involving photoactive quantum dots

* Corresponding author.
* Correspondence to: J. Bujdák, Comenius University in Bratislava, Department of Physical and Theoretical Chemistry, Faculty of Natural Sciences, 842 15 Bratislava, Slovakia.
E-mail addresses: virginia.martinez@ehu.eus (V. Martínez-Martínez), juraj.bujdak@uniba.sk (J. Bujdák).

https://doi.org/10.1016/j.clay.2018.01.001
Received 17 November 2017; Received in revised form 4 January 2018; Accepted 4 January 2018
Available online 06 February 2018

(Kehlbeck et al., 2008). In addition to basic colloids and solids, FRET has also been investigated in well-defined molecular films and self-assemblies, including layer-by-layer assemblies (Bujdák, 2014; Dey et al., 2013), and Langmuir-Blodgett films (Hussain et al., 2010; Hussain and Schoonheydt, 2010; Zhou et al., 2011).

The first study aimed at qualitative comparison between FRET in colloidal and solid materials was carried out for rhodamine dyes intercalated in saponite (Bujdák et al., 2010). Much higher efficiencies were observed for the solid materials, due to the three-dimensional character of the energy transfer. Indeed, the key role of the silicate host is to bring about an optimal distance and molecular orientation between the interacting ED and EA molecules. However, too high a concentration of the molecules could lead to fluorescence quenching caused by dye molecular aggregation (Bujdák et al., 2010), lowering the FRET efficiency. Thus, size-matching rules were adopted to prepare host-guest systems with high concentrations of dye molecules but avoiding molecular aggregation (Egawa et al., 2011). However, this methodology has so far been limited to systems with porphyrin dyes (Eguchi et al., 2014; Ishida et al., 2012). FRET efficiency is also dependent on the ED/EA ratio (Bujdák et al., 2010), although FRET is not limited to a one-step process. Indeed, FRET can be more efficient if proceeding in two or more steps (Bujdák et al., 2011; Saha et al., 2016). In fact, cascade FRET, mimicking a very complex processes occurring in photosynthetic cells, has already been demonstrated in a saponite system intercalated with a mixture of six laser dyes (Belušáková et al., 2015).

The main role of the layered host was to tune the intermolecular distances to increase the FRET efficiency. A first attempt to model the effect of dye/silicate loading on FRET efficiency in colloids was made very recently, in the detailed investigation of (Belušáková et al., 2017). Good agreement between the theoretical model and the experimental values of FRET efficiency was observed. The objective of this work is to build a theoretical model and experimentally characterize FRET in solid samples composed of two laser dyes and an expandable layered silicate, saponite.

2. Experimental methods

2.1. Materials and sample preparation

The synthetic saponite Sumecton SA (Sap) was purchased from Kunimine Industries Co., Ltd., Japan and used as received. The cation exchange capacity (*CEC*) of Sap is 0.72 ± 0.05 mmol g^{-1} (Utracki et al., 2007). Its structural formula is:

$$[(Si_{7.20}Al_{0.80})(Mg_{5.97}Al_{0.03})O_{20}(OH)_4]^{-0.77}(Na_{0.49}Mg_{0.14})^{+0.77}$$

The laser dyes rhodamine 6G (R6G) and oxazine 4 (Ox4) (see Fig. S1 in Supporting information) were purchased from Acros Organics, and used as received. Deionized and purified Milli-Q water was used for the preparation of all colloid samples and aqueous stock solutions.

Concentrations of aqueous stock solutions of the dyes were determined using the Lambert-Beer law after appropriate dilution in ethanol (Belušáková et al., 2017). Molar absorption coefficients are available from the literature (Belušáková et al., 2015). Thin solid films were prepared from the colloids, which had been prepared by mixing the aqueous dye solution(s) and the aqueous Sap colloidal dispersion (Belušáková et al., 2017). The final concentration of each organic dye (c_{dye}) in the colloid precursors was always 6×10^{-7} mol L^{-1}, if not stated otherwise. In the systems containing both dyes, the total dye molar concentration (c_{dyes}) was $2 \times c_{dye} = 1.2 \times 10^{-6}$ mol L^{-1}. The loadings (a_{dyes}, a_{dye}, representing the ratios n_{dyes}/m_{Sap} and n_{dye}/m_{Sap}, respectively) are expressed as percentage of the *CEC* of Sap (%*CEC*). n_{dyes} and n_{dye} are symbols for the amount of dye(s) and m_{Sap} represents the mass of Sap. A variable composition of the colloids with different dye loadings was achieved by changing the Sap concentration and keeping c_{dyes} constant. a_{dyes} values were in the range of 7.2×10^{-7}–7.2×10^{-5} mol g^{-1}, which corresponded to 0.1, 0.2, 0.35, 0.5, 1.0, 5.0 and 10.0%*CEC*, respectively. The loadings of each individual dye (a_{dye}) were half the value of a_{dyes}, being in the range 0.05–5.0%*CEC*. 9 ml colloidal dispersions were used for the preparation of the hybrid films by the vacuum filtration technique (Kawamata et al., 2010), using nitrocellulose membrane filters of < 0.05 μm pore size and 47 mm diameter. After the filtration, films were dried overnight at laboratory temperature. Films left deposited on the membranes were used for all the measurements, unless stated otherwise. The abbreviation of the sample names reflects the dye composition and loading. For example, $Mix_{5.0}$Sap denotes Sap film with the mixture of both the dyes, R6G and Ox4. The number expresses the loading, a_{dyes}, in %*CEC*. $R6G_x$Sap and $Ox4_x$Sap are the names of the hybrid films containing only one dye component (R6G or Ox4) and *x* represents the dye loading in %*CEC*.

2.2. Spectroscopic methods

UV–vis absorption spectra were recorded using a double beam Cary 7000 UV–vis spectrophotometer with an integrating sphere unit (Agilent Technologies). Absorption spectra were recorded in the wavelength range from 350 to 800 nm. Nitrocellulose membranes were recorded as a blank. Results were obtained as %*R* and subsequently transformed to a Kubelka-Munk function (*F*(*R*)) using the Kubelka-Munk transformation method. Steady-state fluorescence emission spectra were recorded using an FLS920 Spectrometer (Edinburgh Instruments) in a front-face configuration with excitation wavelength set to 475 nm. Time-resolved fluorescence (TRF) spectra were recorded in the same spectrometer, using a microchannel plate detector (Hamamatsu C4878) with a picosecond time resolution. Excitation was performed by means of a supercontinuum laser (Fianium) with 150 ps full width at half-maximum (FWHM) pulses. The excitation was set to 470 nm, and TRF was measured at 550 nm for the ED (R6G) and 650 nm for the EA (Ox4). Samples based on EA (Ox4) fluorophores alone were characterized with excitation and emission wavelengths set to 585 and 650 nm, respectively. The corresponding lifetimes τ were obtained using exponential reconvolution fitting functions (FAST software). The deconvolution process was evaluated by the chi-square χ^2 statistical parameter and residuals analysis. The χ^2 values were in the range of $0.9 < \chi^2 < 1.3$, and higher-order exponential fits were accordingly chosen as the most appropriate for the major part of the calculations. The average lifetime $\bar{\tau}$ was then calculated using Eq. (1), where τ_i represents the *i*-th fractional lifetime obtained from the *k*-th order reconvolution fit and α_i is the corresponding *i*-th lifetime fractional intensity:

$$\bar{\tau} = \sum_{i=1}^{k} \alpha_i \tau_i \quad (1)$$

FRET efficiency was calculated from the results of TRF according to Eq. (2), where τ_{ED+EA} and τ_{ED} represent the lifetimes of the energy donor in the presence and in the absence of the energy acceptor, respectively:

$$E = 1 - \frac{\tau_{ED+EA}}{\tau_{ED}} \quad (2)$$

2.3. Model for the calculation of FRET efficiency

A similar approach to that described in our recent study dealing with FRET in colloidal systems (Belušáková et al., 2017) has been adopted. The model applied in this work is based on the phenomenon occurring in a three-dimensional matrix. Since FRET between the interacting molecules depends primarily on their intermolecular distance, the molecular distribution plays a key role in the FRET efficiency estimation. Structural constraints due to the presence of lamellar particles

were neglected to simplify the model. The thickness of the fundamental particles of Sap (0.96 nm) is much lower than the Förster radius for the ED/EA pair (R_0 = 5.64 nm) (Belušáková et al., 2017), so the distribution of the dye molecules was modeled as if in a homogeneous, three-dimensional solid. Considering the value of the Förster radius, FRET would be near 100% at distances of $r < 5$ nm. FRET can proceed in any direction, including along the surface, or perpendicular to the layers of silicate particles. FRET would be considerably reduced at distances significantly higher than R_0. As the Förster radius between R6G and Ox4 is 5.64 nm and the basal spacing of the films is around 1.3 nm, FRET should be highly efficient up to four interlayer cavities away (on both sides) from the interlayer space. The mean intermolecular distance would not be a suitable parameter to describe FRET due to the non-centrosymmetric function of FRET efficiency (Belušáková et al., 2017):

$$E(\mathrm{r}) = \frac{R_0^6}{R_0^6 + r^6} \tag{3}$$

The probability function of the distance r between the interacting molecules was defined as a function of dye molecule concentration (σ_N). The probability of the separation between the nearest molecules in space was characterized using a probability density function $f(r, \sigma_N)$ expressed by a Poisson probability distribution (Zwillinger, 2003). The parameter r is an independent variable defined as the distance between ED and EA molecules in three-dimensional space ($0 < r < \infty$). $f(r, \sigma_N)$ depends on the parameter of the average number concentration (that is, concentration in terms of number of molecules per unit volume) σ_N. Since $f(r, \sigma_N)$ describes the distribution of dye molecules, it is of significant interest for the characterization of FRET efficiency:

$$f(r, \sigma_N) = 4\pi\sigma_N(\mathrm{EA})r^2 \mathrm{e}^{-\frac{4}{3}\sigma_N(\mathrm{EA})\pi r^3} \tag{4}$$

Only FRET from the ED to the nearest EA molecule was considered in the model. FRET to the second- or third-nearest EA molecule was neglected, since its efficiency would always be much lower. The FRET efficiency between the ED and EA molecules, $E(r)$, can be defined as a function of the intermolecular distance r and depends only on the parameter R_0, representing the Förster radius for R6G and Ox4 (see Eq. (3)). The expected value of the FRET efficiency $\overline{E}$ for a specific loading of dye molecules was calculated by integration of the inner product of the probability density function $f(r, \sigma_N)$ and the function for the FRET efficiency $E(r)$ using Eq. (5):

$$\overline{E} = \int_{r=0}^{\infty} E(r) f(r, \sigma_N) \mathrm{d}r \tag{5}$$

The integration was performed only up to a limit of 40 nm, due to the negligible contributions of both $f(r, \sigma_N(\mathrm{EA}))$ and $E(r)$ at larger r values. The molar mass of Sap was calculated from its structural formula, giving a value of 772 g mol^{-1} (Belušáková et al., 2017). Using the theoretical structural unit dimension parameters for saponite, a = 5.33 10^{-10} m, b = 9.23 10^{-10} m, and c = 9.6 10^{-10} m (Suquet et al., 1975), the structural unit volume would be 0.472 nm^3. The density of the layer can be calculated from the unit molar mass (M_{unit}) and volume (V_{unit}):

$$\rho = \frac{M_{\mathrm{unit}}}{V_{\mathrm{unit}} N_A} \tag{6}$$

The theoretical value of 2.71 g cm^{-3} was corrected for the presence of hydrated interlayer spaces in swollen saponite. The thickness of the interlayer spaces was calculated as the difference between the basal spacing d_{001} and the thickness of a single layer (0.96 nm). The density of the hydrated interlayer spaces is considered to be approximately the same as that of liquid water (1.0 g cm^{-3}). Deviations due to the presence of inorganic or dye cations were neglected. The number density of EA molecules (σ_N(EA)) and average intermolecular distances were also calculated.

Table 1
Characteristic parameters of solid films based on mixtures of rhodamine 6G and oxazine 4 intercalated in saponite: dye-loadings in %*CEC*.

a_{dyes}/%*CEC*	d_{001}/nm	σ/g cm^{-3}	a_{EA}/mmol g^{-1}	σ_N(EA)/nm^{-3}	$\overline{d}$/nm
0.10	1.31	2.25	3.55 × 10^{-4}	4.82 × 10^{-4}	16.1
0.20	1.33	2.23	7.10 × 10^{-4}	9.55 × 10^{-4}	12.8
0.35	1.36	2.21	1.25 × 10^{-3}	1.65 × 10^{-3}	10.7
0.5	1.37	2.20	1.78 × 10^{-3}	2.35 × 10^{-3}	9.48
1.0	1.39	2.18	3.55 × 10^{-3}	4.66 × 10^{-3}	7.54
5.0	1.41	2.16	1.78 × 10^{-2}	2.31 × 10^{-2}	4.42
10.0	1.41	2.16	3.55 × 10^{-2}	4.63 × 10^{-2}	3.51

d_{001} – basal spacings, σ - theoretical densities of saponite materials corrected by the presence of hydrated interlayer spaces, a_{EA} - loading of EA molecules, σ_N(EA) - number density of EA dye molecules (which is half the value of the total number density of both dyes), $\overline{d}$ - average distance between homogeneously distributed molecules in space (assuming ordered cubic packing).

3. Results and discussion

3.1. Photophysical characterization of the samples

R6G and Ox4 played the role of ED and EA, respectively. The selection of these dyes was based on the significant overlap between the emission spectrum of the ED and the absorption spectrum of the EA (Fig. S1). Regarding the theoretical model described above, it was found that a very low a_{EA} was sufficient to reach high FRET efficiencies. Indeed, in agreement with previous studies (Bujdák et al., 2010), the necessary concentration is almost ten times lower for the solid state samples than that required for the two-dimensional FRET process in colloidal systems (Belušáková et al., 2017). This is reflected in our choice of range of a_{EA} values to study (see Table 1).

The absorption spectrum of the Mix$_{0.1}$Sap film showed the presence of both of the dyes (Fig. 1A). The main absorption band of R6G$_{0.05}$Sap, centered at 550 nm, was red-shifted with respect to that in the spectrum recorded for dye solution (Fig. S1), and similar to the spectra obtained for R6G/Sap colloids (Belušáková et al., 2015; Belušáková et al., 2017). The R6G spectra changed significantly for the samples with high dye loading (R6G$_{5.0}$Sap) and a new blue-shifted band at around 520 nm appeared (Fig. 1B, Fig. 2A). Note that this change was also observed in the spectra of the Mix$_x$Sap films, as represented by the spectrum of the sample with the highest dye loading, Mix$_{10.0}$Sap (Fig. 1B). On the other hand, the spectral profiles of Ox4 did not exhibit significant variations over the sample series (Fig. 1A, B). The spectra of adsorbed Ox4 were partially different from that obtained for the solution (Fig. S1), but a similar change was also observed for Ox4/smectite colloids in previous studies (Bujdák, 2014; Belušáková et al., 2017).

The new band at the lower wavelengths in the R6G spectra was assigned to H-aggregates. Since H-aggregates are non-luminescent, and are very efficient fluorescence quenchers, fluorescence spectroscopy was the obvious method for verifying the presence of R6G molecular aggregates in the films. In this regard, the emission spectra of R6G/Sap films did not show much variation between dye loadings of 0.05 and 0.5%*CEC* (Fig. 2B). However, significant fluorescence quenching was observed for films with higher loadings, R6G$_{2.5}$Sap and R6G$_{5.0}$Sap, where the intensity of the main band, centered at around 570 nm, was significantly reduced (sample R6G$_{2.5}$Sap, Fig. 2B), or practically negligible (sample R6G$_{5.0}$Sap, Fig. 2B). The decrease in fluorescence could be explained by the formation of H-type assemblies, which are generally formed at high concentrations. Interestingly, in these two samples a new blue-shifted band, located at about 540 nm, was observed in the emission spectra. Its relevance was confirmed by chemometric analysis (Lofaj et al., 2013), where two significant spectral components were identified (Fig. S2). Although the diminution of fluorescence clearly indicates the presence of molecular aggregates, the emission at 540 nm cannot be assigned to photoactive H-dimers. If another type of luminescent aggregates was formed, the aggregates would emit at lower

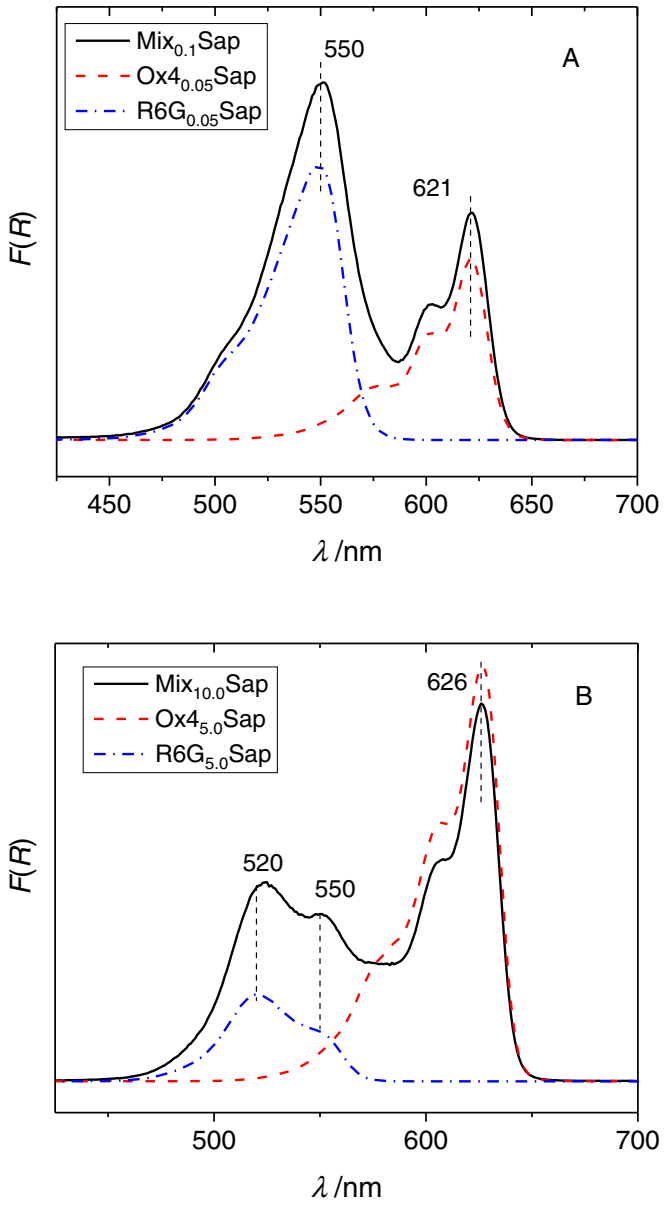

Fig. 1. Absorption spectra of the films prepared from saponite colloids with rhodamine 6G, oxazine 4, or a mixture of the two, with 0.1%*CEC* (A) and 10%*CEC* (B) loading.

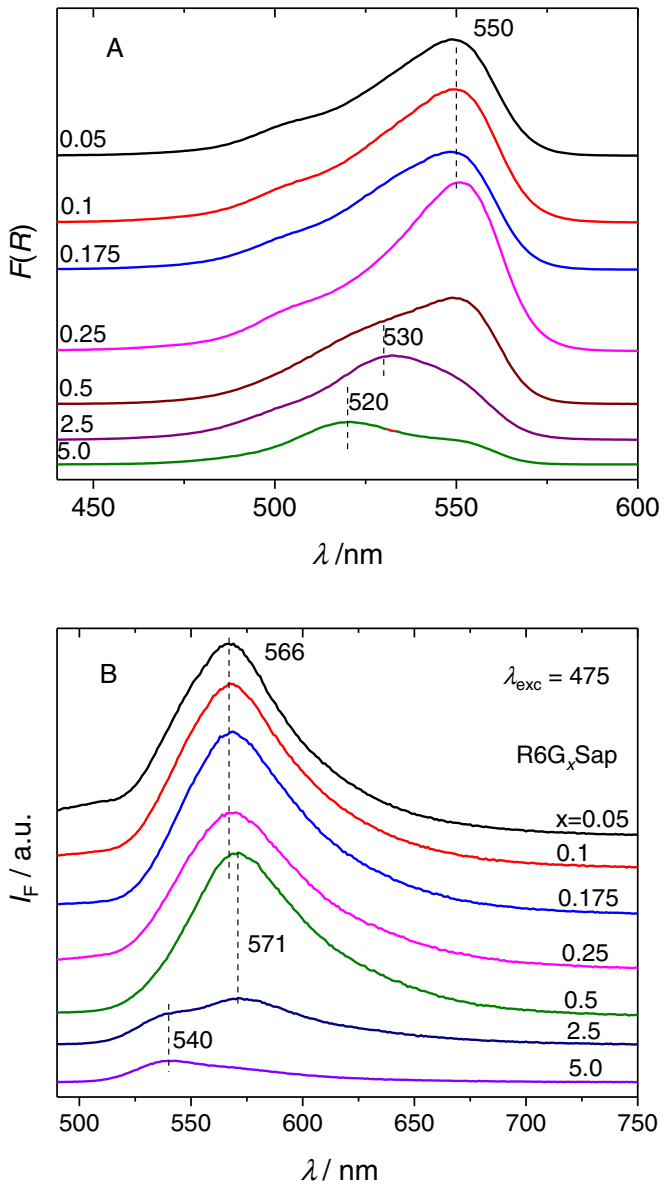

Fig. 2. Absorption (A) and emission spectra (B) of rhodamine 6G/saponite hybrid films with different dye loadings.
Loadings are expressed in %*CEC*. Vertical dashed lines denote the positions of spectral bands. Numbers near dashed lines denote the maxima of the spectral bands.

energies according to the Kasha rules (Kasha et al., 1965). Probably the species emitting at 540 nm are the same ones absorbing light at 520 nm (Figs. 1B, 2A), and might have coexisted with the H-aggregates. The identity of the 540 nm emitter is unknown, although similar properties have been found for some rhodamine dyes in other studies (Sas et al., 2017; Sasai et al., 2011). De-alkylation of rhodamine dyes under strong irradiation can be detected by shifts of the absorption and emission bands to lower wavelengths (Wang et al., 2014): the products of the de-alkylation reaction would be rhodamine dyes with NH_2 groups, with light absorption approaching 500 nm. Another possible scenario leading to the same spectral changes would be a distortion of the R6G molecular skeleton, disrupting the planarity of the structure. In such a case, a very small deformation of the chromophores would lead to a reduced area of π-electron delocalization, which would be reflected in blue-shifts of the spectral bands, together with a decrease of fluorescence yields. Note here that a more perpendicular arrangement with respect to the plane of the silicate layers is typically observed at high dye loading in several homologous systems (Bujdák and Iyi, 2005, 2006; Bujdák et al., 2003; Bujdák et al., 2007; Hoppe et al., 1997; Iyi et al., 2002; López Arbeloa and Martínez Martínez, 2006; Martínez Martínez et al., 2005; Sasai et al., 2002). Our hypothesis is that in such an orientation, the -NHC_2H_5 groups of R6G cations (bearing a partial positive charge) could interact with basal oxygen atoms of the opposite layers. This partial fitting of the -NHC_2H_5 groups into the ditrigonal holes would impose a structural constraint causing a slight deviation in the planarity of chromophoric skeleton. There are several examples of the molecular structure of a dye being altered upon intercalation, which in most cases leads to significant changes of the dye's spectral properties (Bujdák et al., 2016; Sonotani et al., 2017; Takagi et al., 2013; Tsukamoto et al., 2016).

For Mix_xSap films, the FRET process between ED (R6G) and EA (Ox4) showed predictable tendencies for samples with a dye loading of < 5%*CEC* (Fig. 3). The spectrum of the $Mix_{0.1}$Sap film, after selective excitation of R6G at 475 nm, shows a significant decrease of the R6G emission in favor of Ox4 fluorescence. In fact, the R6G and Ox4 emission bands were similar in intensity, indicating that a significant part of the excitation energy was transferred from R6G to Ox4. In the case of

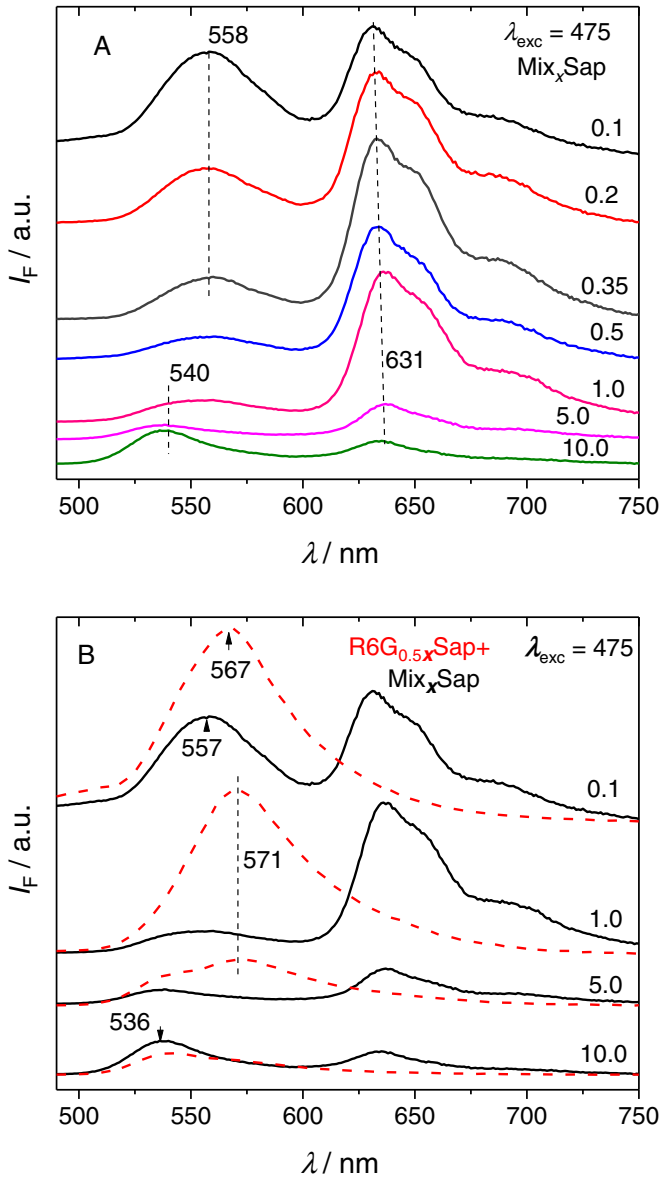

Fig. 3. The emission spectra of the films of saponite containing a mixture of rhodamine 6G and oxazine 4 dyes.
A: The spectra obtained for different loadings. B: Comparison of the emission spectra of the systems containing a mixture of energy donor and acceptor (solid lines) and those with the energy donor alone (dashed lines). Different loadings expressed in %*CEC* are placed as numerical values at ends of the spectra. The vertical dashed lines and corresponding numbers at their positions have the same meaning as in Fig. 2.

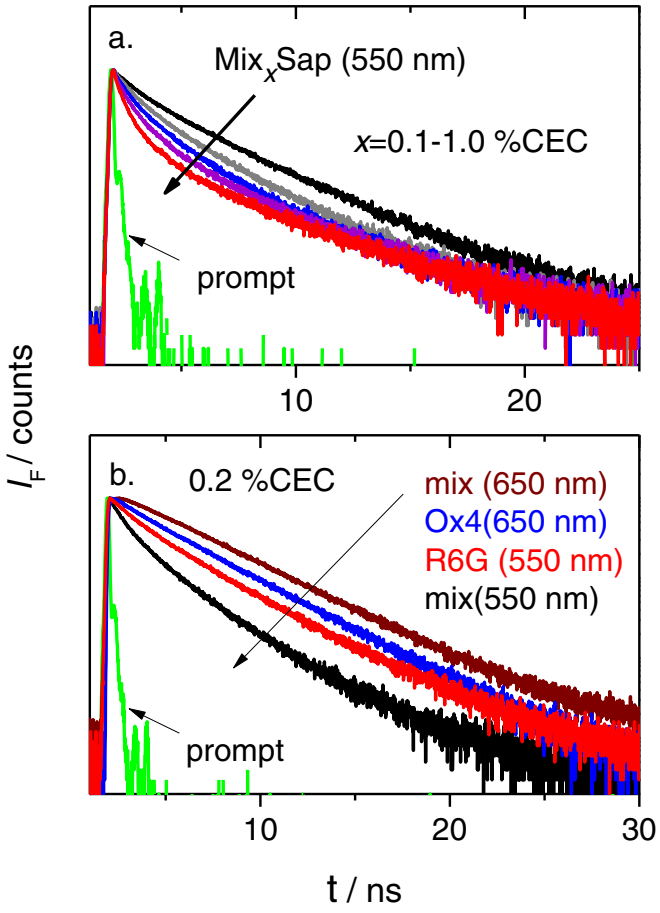

Fig. 4. Time-resolved fluorescence profiles of selected films.
a. The effect of dye loading: 0.1, 0.2, 0.35, 0.5, 1.0%*CEC*. The emission from rhodamine 6G molecules was recorded selectively at 550 nm. b. The profiles recorded at 550 nm were compared for the Mix$_{0.2}$Sap (mix) and R6G$_{0.1}$Sap (R6G) films.

1%*CEC*, the R6G emission band almost disappeared in favor of the Ox4 fluorescence band (Fig. 3), which confirms almost 100% FRET efficiency. At this loading no significant degree of molecular aggregation of the dye is expected, nor does it seem to be present, to judge by the strong R6G fluorescence from the corresponding R6G$_{0.5}$Sap film (Fig. 3B). Moreover, the excitation spectra of the films Mix$_{0.1}$Sap and Mix$_{1.0}$Sap (taken as representative) also show the efficient occurrence of FRET (Fig. S3). However, for dye loadings over 1%*CEC*, the overall fluorescence was much lower, indicating a strong quenching by molecular aggregates in a similar way as in the films based on single dye components at the same loading (Fig. 2B, Figs. S4, S5). Remarkably, some emission at low wavelengths (540 nm) was exhibited in Mix$_{5.0}$Sap and Mix$_{10.0}$Sap, similar to that already observed for R6G$_{5.0}$Sap film (Fig. 2B). In these samples, the presence of another R6G species emitting at lower wavelengths complicates the evaluation of FRET efficiency. However, these luminescent species emitting at about 535–540 nm seem to be sensitive to neither FRET nor fluorescence quenching (Fig. 3). Although the spectral overlap between ED and EA should be lower for this species, that alone should not completely suppress the FRET process between them. One possible explanation is relative orientation: if the unknown R6G species has perpendicular orientation relative to the saponite layers, and Ox4 has planar orientation, the orientation factor κ^2 will be less favorable for FRET ($\kappa^2 = 0$) if the dipole moments between ED and EA are oriented perpendicular to each other (Lakowicz, 2006).

FRET efficiency can be determined directly from the steady-state fluorescence spectra by comparison of the emission from the film with only the ED with that of the film containing both the ED and EA (Fig. 3B). However, a more accurate way is to use TRF, which reflects the kinetics of the relaxation processes. For this reason we calculated FRET efficiency by comparing the TRF of ED alone with the data of the mixed system containing both the ED and EA. The quenching of ED fluorescence in Mix$_x$Sap films increased with dye loading, observable as a steeper decline in the decay curve (Fig. 4A). The shortening of the lifetimes in R6G$_x$Sap samples with high dye loading (from 2.22 ns to 1.5 ns) is due to both energy migration and self-quenching after reaching sites occupied by molecular aggregates. Nevertheless, the quenching due to FRET in mixed-dye systems in the range 0.35–1.0%*CEC* was much more efficient than the self-quenching in the films with ED alone. The fluorescence decay profiles of the R6G$_{0.1}$Sap and Mix$_{0.2}$Sap films are compared in Fig. 4B. The decay recorded at ED emission maximum (550 nm) was significantly faster in the Mix$_{0.2}$Sap

Table 2
Fluorescence lifetimes of R6G in the presence ($\tau_{ED + EA}$) and absence (τ_{ED}) of Ox4 in thin solid films, χ^2 values of the fits, and FRET efficiency (E_{FRET}) as calculated from the theoretical model and as determined by time-resolved fluorescence spectroscopy.

a_{dyes}/%*CEC*	τ_{ED}/ns	χ^2	$\tau_{ED + EA}$/ns	χ^2	E_{FRET}/%	
					Theoretical	TRF
0.1	2.22	1.138	1.74	1.142	35	28
0.2	2.23	1.137	1.22	1.148	53	48
0.35	1.87	1.097	0.98	1.235	68	52
0.5	1.68	1.174	0.72	1.273	77	56
1	1.49	1.143	0.55	1.254	90	70
5	1.40	1.186	0.79	1.448	99	52
10	1.68	1.169	1.49	1.363	100	23

Average lifetime values were calculated using Eq. (1). τ values were obtained using three-exponential fits.

film. In fact, the ED lifetime of Mix$_x$Sap films changed from 1.74 to 0.55 ns when the dye loading increased from 0.1 to 1%*CEC* (Table 2). The shortest lifetimes recorded at 550 nm were expected in the films with the highest loadings, where the probability of either self-quenching, FRET, or both, should be highest. However, according to the lifetimes, the self-quenching in R6G$_x$Sap films was highest at 5%*CEC* loading, with a lifetime of 1.40 ns (Table 2). Concerning the mixed dye systems, the lowest lifetime at 550 nm was observed for the Mix$_{1.0}$Sap film (0.55 ns), indicating that in this case FRET has the highest efficiency. However, the longer lifetime observed for the sample with the highest loading, the Mix$_{10.0}$Sap film (1.49 ns), indicates that there, the relaxation of the species emitting at 550 nm was inefficiently quenched by the EA molecules. These results are complementary to those observed by steady-state fluorescence, which confirm that the samples with the highest R6G loadings (5.0%*CEC*) do not photophysically interact with either EA or the molecular aggregates. The possible nature of this species was discussed earlier.

3.2. FRET efficiency calculation

As depicted in Table 1, increasing the dye loading decreases the average distance between neighboring dye molecules, $\overline{d}$. Samples can be divided into three groups:

i. Samples with 0.1–0.5%*CEC* loadings characterized by $\overline{d} \gg R_0$.
ii. Films with 1.0 and 5.0%*CEC* loadings having $\overline{d}$ values similar to R_0.
iii. The sample Mix$_{10.0}$Sap in which $\overline{d} \ll R_0$.

Note here that the average intermolecular distance as calculated from the average density of the molecules is not an optimal parameter for the estimation of FRET efficiency. The argument is similar to that reported recently in our study on FRET occurring in dyes/layered silicate colloids (Belušáková et al., 2017). The $\overline{d}$ value reflects the distance between dye molecules under the conditions of a periodically-ordered distribution of dye molecules in space. Applying such a model in a three-dimensional system leads to several molecules of EA surrounding each ED molecule, depending on the distribution of dye molecules used in the model. It is more realistic to base a model on a heterogeneous distribution, with a statistical distribution of the molecules in space, in which intermolecular distances both above and below $\overline{d}$ would occur. Therefore, we applied a model based on a Poisson distribution of molecules in three-dimensional space to estimation of FRET efficiency. The probability density functions were calculated for the parameter *r*, which represents the intermolecular distance between an ED molecule with a fixed position in space and the nearest EA molecule. These functions describe the statistical distribution of the intermolecular distances, which depends on the average concentration of EA molecules. The most probable distances occurring for each system are shown as the maxima of the respective probability density functions (Fig. 5), which are

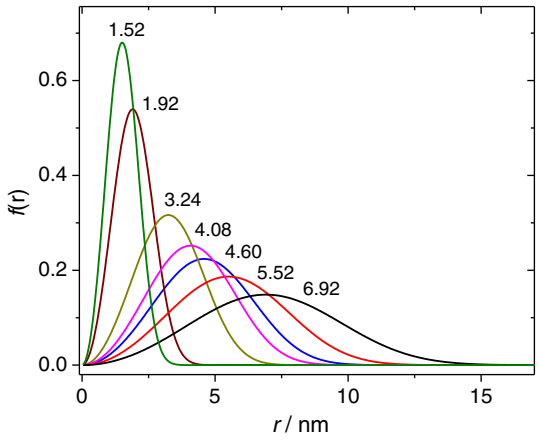

Fig. 5. The probability density functions of the variable *r*, representing the distance between the energy donor and closest energy acceptor.
The numbers denote the distance *r* with highest probability density for a particular loading. The functions and their maxima correspond (from left to right) to the loadings: 10.0, 5.0, 1.0, 0.5, 0.35, 0.2, 0.1%*CEC*.

indeed much lower than the $\overline{d}$ values (Table 1), as a consequence of the fact that the $\overline{d}$ parameter is derived from a model of periodically-distributed molecules in a perfectly ordered system. A similar trend was observed for FRET in two-dimensional systems (Belušáková et al., 2017). The maximum of the probability density function (for the nearest molecule) is always equal to or lower than the $\overline{d}$ value, due to the nature of the two parameters. A very high FRET efficiency value would be expected for the Mix$_{1.0}$Sap sample (Fig. 6), in which only a very small fraction of the EA molecules have $r > R_0$ (*r* is most probable at 3.24 nm) (Fig. 5). In the same vein, the samples Mix$_{0.5}$Sap and Mix$_{0.35}$Sap would still exhibit a most probable intermolecular distance *r* lower than the R_0 value (4.08 and 4.60 nm), but a significant fraction of the probability distribution would still be at larger values. Mix$_{0.2}$Sap would have a most probable distance *r* (5.52 nm) very close to R_0, and Mix$_{0.1}$Sap was the only sample with a most probable value of intermolecular distance (6.92 nm) larger than R_0 (Fig. 6). Thus for the two samples of the lowest loading, FRET efficiency would be expected to be near and < 50%, respectively. This was only a rough estimation, since the expected values of the FRET efficiencies are obtained by the integration of the inner product of the probability distribution function *f* (*r*) and the function describing FRET efficiency between two ED and EA molecules in dependence on *r* (Eq. (5)). The theoretical FRET efficiency values can be read off at large *r*, where the resulting value of the inner

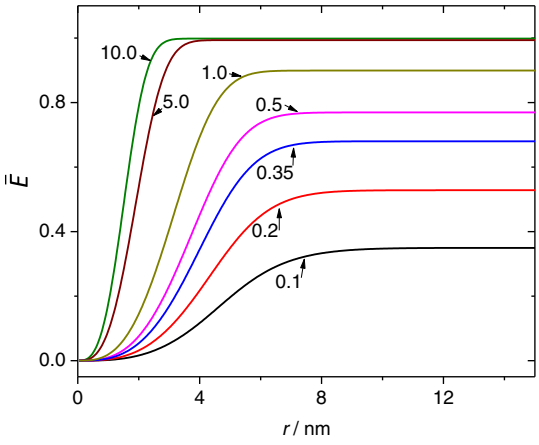

Fig. 6. Calculated values of the theoretical FRET efficiencies and their dependence on the *r* value taken as the integration limit.
The constant value at larger *r* distances shows that the FRET contribution at these distances converges to zero. The numbers with arrows denote dye loadings (in % *CEC*).

product does not change any more and approaches a limiting value.

The expected values of FRET efficiencies, according to our model, are summarized in Table 2. For $Mix_{0.1}$Sap and $Mix_{0.2}$Sap, the calculated theoretical efficiency value reaches 35% and 53% respectively, a result that is in a good agreement with the values estimated experimentally (28% and 48%). Although based on the theory, a maximum FRET efficiency of 100% was expected for the samples with 10.0 and 5.0%*CEC* loadings, this was not found experimentally. This is because the theoretical values were determined for idealized conditions. However, the presence of the R6G species, which retains relatively strong fluorescence even in the mixed-dye samples at high loadings, makes the FRET efficiency unpredictable. The effect of this species was already observed at relatively low loadings (0.35, 0.5, 1.0%*CEC*) as shown by the reduced experimental values of FRET yields with respect to the theoretical values (Table 2). As mentioned before, the specific orientation of the R6G molecules forming these species plausibly explains the observed decrease in FRET efficiency with increasing dye loading, as well as the lower FRET values obtained for these films.

4. Conclusions

As the dye loading increased in Mix_xSap films, the FRET efficiency between ED (R6G) and EA (Ox4) also increased, up to a loading of 1%*CEC*, at which FRET efficiency attained maximal values. Above this value, fluorescence was significantly quenched, probably due to the presence of molecular aggregates of the dye. The exception was the emission signal of a new blue-shifted R6G species, which seemed neither to be quenched by the H-aggregates nor to take part in the FRET process. The identity of this species is not clear yet, but is hypothesized to be the R6G species with distorted planarity and oriented perpendicular to the Sap layers (as the probability of energy transfer between molecules with transition moments perpendicular to each other is zero). We proposed a theoretical model for estimation of FRET efficiency, based on statistical distribution of the molecules in the three dimensional interior of the solid, which works reasonably well for Mix_xSap films with low dye loading ($\leq$ 1%*CEC*). When comparing experimental values with theory, the very sensitive relation of FRET efficiency to dye intermolecular distances (being a function of r^6) should be considered. At higher dye loading, the dye aggregation or the formation of new rhodamine 6G species makes the theoretical prediction more complicated and the results are not in such good agreement with the experimental data. Under these conditions, either other phenomena influence the properties of adsorbed dye, or there occurs the formation of dye aggregates which compete with EA molecules in the process of fluorescence quenching. Future work will focus on the investigation of new hybrid solid systems. Other pairs of energy donor and acceptors will be sought, and reaction conditions optimized, in order to test and refine our theoretical model for higher dye/layered silicate loadings.

Acknowledgements

This work was supported by the Slovak Research and Development Agency under contract No. APVV-15-0347, APVV-15-0741. Acknowledgements are due to The National Scholarship Programme of the Slovak Republic, which supported the research stay of SB at University of the Basque Country (Bilbao, Spain). Supports from the VEGA Grant Agency (1/0278/16) and Comenius University Grant GUK (UK/303/2016) are also gratefully acknowledged. Financial support was given by the Basque Government (IT912-16) and Ministerio de Economía y Competitividad “MINECO” (MAT2017-83856-C3-3-P).

Appendix A. Supplementary data

Supplementary data to this article can be found online at https://doi.org/10.1016/j.clay.2018.01.001.

References

Belušáková, S., Lang, K., Bujdák, J., 2015. Hybrid systems based on layered silicate and organic dyes for cascade energy transfer. J. Phys. Chem. C 119, 21784–21794.
Belušáková, S., Martínez-Martínez, V., Arbeloa, I.L., Bujdák, J., 2017. Resonance energy transfer between dye molecules in colloids of a layered silicate. The effect of dye surface concentration. J. Phys. Chem. C 121, 8300–8309.
Bujdák, J., 2014. Layer-by-layer assemblies composed of polycationic electrolyte, organic dyes, and layered silicates. J. Phys. Chem. C 118, 7152–7162.
Bujdák, J., Iyi, N., 2005. Molecular orientation of rhodamine dyes on surfaces of layered silicates. J. Phys. Chem. B 109, 4608–4615.
Bujdák, J., Iyi, N., 2006. Spectral and structural characteristics of oxazine 4/hexadecyltrimethylammonium montmorillonite films. Chem. Mater. 18, 2618–2624.
Bujdák, J., Iyi, N., Kaneko, Y., Czímerová, A., Sasai, R., 2003. Molecular arrangement of rhodamine 6G cations in the films of layered silicates: the effect of the layer charge. Phys. Chem. Chem. Phys. 5, 4680–4685.
Bujdák, J., Martinez, V.M., Arbeloa, F.L., Iyi, N., 2007. Spectral properties of rhodamine 3B adsorbed on the surface of montmorillonites with variable layer charge. Langmuir 23, 1851–1859.
Bujdák, J., Chorvát, D., Iyi, N., 2010. Resonance energy transfer between rhodamine molecules adsorbed on layered silicate particles. J. Phys. Chem. C 114, 1246–1252.
Bujdák, J., Czímerová, A., Arbeloa, F.L., 2011. Two-step resonance energy transfer between dyes in layered silicate films. J. Colloid Interface Sci. 364, 497–504.
Bujdák, J., Ratulovská, J., Donauerová, A., Bujdáková, H., 2016. Hybrid materials based on luminescent alkaloid berberine and saponite. J. Nanosci. Nanotechnol. 16, 7801–7804.
Calzaferri, G., 2008. Energy transfer in nanochannels. IL Nuovo Cimento B 123, 1337–1367.
Dey, D., Bhattacharjee, D., Chakraborty, S., Hussain, S.A., 2013. Effect of nanoclay laponite and pH on the energy transfer between fluorescent dyes. J. Photochem. Photobiol. A 252, 174–182.
Diacon, A., Rusen, E., Boscornea, C., Zaharia, C., Cincu, C., 2010. Hybrid dye sensitized solar cells. J. Optoelectron. Adv. Mater. 12, 199–204.
Egawa, T., Watanabe, H., Fujimura, T., Ishida, Y., Yamato, M., Masui, D., Shimada, T., Tachibana, H., Yoshida, H., Inoue, H., Takagi, S., 2011. Novel methodology to control the adsorption structure of cationic porphyrins on the clay surface using the "size-matching rule". Langmuir 27, 10722–10729.
Eguchi, M., Watanabe, Y., Ohtani, Y., Shimada, T., Takagi, S., 2014. Switching of energy transfer reaction by the control of orientation factor between porphyrin derivatives on the clay surface. Tetrahedron Lett. 55, 2662–2666.
Epelde-Elezcano, N., Martínez-Martínez, V., Duque-Redondo, E., Temiño, I., Manzano, H., López-Arbeloa, I., 2016. Strategies for modulating the luminescence properties of pyronin y dye-clay films: an experimental and theoretical study. Phys. Chem. Chem. Phys. 18, 8730–8738.
Fujii, K., Kuroda, T., Sakoda, K., Iyi, N., 2011. Fluorescence resonance energy transfer and arrangements of fluorophores in integrated coumarin/cyanine systems within solid-state two-dimensional nanospace. J. Photochem. Photobiol. A 225, 125–134.
Giovanella, U., Leone, G., Galeotti, F., Mroz, W., Meinardi, F., Botta, C., 2014. FRET-assisted deep-blue electroluminescence in intercalated polymer hybrids. Chem. Mater. 26, 4572–4578.
Hoppe, R., Alberti, G., Costantino, U., Dionigi, C., Schulz-Ekloff, G., Vivani, R., 1997. Intercalation of dyes in layered zirconium phosphates. 1. Preparation and spectroscopic characterization of alpha-zirconium phosphate crystal violet compounds. Langmuir 13, 7252–7257.
Hussain, S.A., Schoonheydt, R.A., 2010. Langmuir-Blodgett monolayers of cationic dyes in the presence and absence of clay mineral layers: *N,N* '-dioctadecyl thiacyanine, octadecyl rhodamine B and laponite. Langmuir 26, 11870–11877.
Hussain, S.A., Chakraborty, S., Bhattacharjee, D., Schoonheydt, R.A., 2010. Fluorescence resonance energy transfer between organic dyes adsorbed onto nano-clay and Langmuir-Blodgett (LB) films. Spectrochim. Acta A 75, 664–670.
Ishida, Y., Masui, D., Tachibana, H., Inoue, H., Shimada, T., Takagi, S., 2012. Controlling the microadsorption structure of porphyrin dye assembly on clay surfaces using the "size-matching rule" for constructing an efficient energy transfer system. ACS Appl. Mater. Interfaces 4, 811–816.
Iyi, N., Sasai, R., Fujita, T., Deguchi, T., Sota, T., López Arbeloa, F., Kitamura, K., 2002. Orientation and aggregation of cationic laser dyes in a fluoromica: polarized spectrometry studies. Appl. Clay Sci. 22, 125–136.
Kasha, M., Rawls, H.R., El-Bayoumi, M.A., 1965. The exciton model in molecular spectroscopy. Pure Appl. Chem. 11, 371–392.
Kawamata, J., Suzuki, Y., Tenma, Y., 2010. Fabrication of clay mineral-dye composites as nonlinear optical materials. Philos. Mag. 90, 2519–2527.
Kehlbeck, J.D., Hagerman, M.E., Cohen, B.D., Eliseo, J., Fox, M., Hoek, W., Karlin, D., Leibner, E., Nagle, E., Nolan, M., Schaefer, I., Toney, A., Topka, M., Uluski, R., Wood, C., 2008. Directed self-assembly in laponite/CdSe/polyaniline nanocomposites. Langmuir 24, 9727–9738.
Kuroda, T., Fujii, K., Sakoda, K., 2010. Ultrafast energy transfer in a Multichromophoric layered silicate. J. Phys. Chem. C 114, 983–989.
Lakowicz, J.R., 2006. Principles of Fluorescence Spectroscopy, 3rd ed. Springer, New York.
Li, H.R., Devaux, A., Ruiz, A.Z., Calzaferri, G., 2006. Electronic excitation energy transfer from dye-loaded zeolite L monolayers to a semiconductor. Nano 6195 (61951G-1–61951G-5).
Lofaj, M., Valent, I., Bujdák, J., 2013. Mechanism of rhodamine 6G molecular aggregation in montmorillonite colloid. Cent. Eur. J. Chem. 11, 1606–1619.
López Arbeloa, F., Martínez Martínez, V., 2006. Orientation of adsorbed dyes in the

interlayer space of clays. 2 fluorescence polarization of rhodamine 6G in laponite films. Chem. Mater. 18, 1407–1416.
Martínez Martínez, V., Arbeloa, F.L., Prieto, J.B., Arbeloa, I.L., 2005. Orientation of adsorbed dyes in the interlayer space of clays. 1. Anisotropy of rhodamine 6G in Laponite films by vis-absorption with polarized light. Chem. Mater. 17, 4134–4141.
Neumann, M.G., Oliveira, H.P.M., Cione, A.P.P., 2002. Energy transfer between aromatic hydrocarbons dissolved in a C18-surfactant layer adsorbed on laponite. Adsorption 8, 141–146.
Olivero, F., Carniato, F., Bisio, C., Marchese, L., 2014. Promotion of forster resonance energy transfer in a saponite clay containing luminescent polyhedral oligomeric silsesquioxane and rhodamine dye. Chem. Asian. J. 9, 158–165.
Saha, J., Dey, D., Roy, A.D., Bhattacharjee, D., Hussain, S.A., 2016. Multi step FRET among three laser dyes pyrene, acriflavine and rhodamine B. J. Lumin. 172, 168–174.
Sapsford, K.E., Berti, L., Medintz, I.L., 2004. Fluorescence resonance energy transfer - concepts, applications and advances. Minerva Biotecnol. 16, 247–273.
Sas, S., Danko, M., Bizovská, V., Lang, K., Bujdák, J., 2017. Highly luminescent hybrid materials based on smectites with polyethylene glycol modified with rhodamine fluorophore. Appl. Clay Sci. 138, 25–33.
Sasai, R., Fujita, T., Iyi, N., Itoh, H., Takagi, K., 2002. Aggregated structures of rhodamine 6G intercalated in a fluor-taeniolite thin film. Langmuir 18, 6578–6583.
Sasai, R., Iyi, N., Kusumoto, H., 2011. Luminous change of rhodamine 3B incorporated into titanate nanosheet/decyltrimethylammonium hybrids under humid atmosphere. Bull. Chem. Soc. Jpn. 84, 562–568.
Sonotani, A., Shimada, T., Takagi, S., 2017. "size-matching effect" in a cationic porphyrin-titania nanosheet complex. Chem. Lett. 46, 499–501.
Suquet, H., de la Calle, C., Pezerat, H., 1975. Swelling and structural organization of saponite. Clays Clay Miner. 23, 1–2 (IN1-IN3,3-9).
Takagi, S., Shimada, T., Ishida, Y., Fujimura, T., Masui, D., Tachibana, H., Eguchi, M., Inoue, H., 2013. Size-matching effect on inorganic nanosheets: control of distance, alignment, and orientation of molecular adsorption as a bottom-up methodology for nanomaterials. Langmuir 29, 2108–2119.
Tsukamoto, T., Shimada, T., Takagi, S., 2016. Photophysical properties and adsorption behaviors of novel tri-cationic boron(III) subporphyrin on anionic clay surface. ACS Appl. Mater. Interfaces 8, 7522–7528.
Utracki, L.A., Sepehr, M., Boccaleri, E., 2007. Synthetic, layered nanoparticles for polymeric nanocomposites (PNCs). Polym. Adv. Technol. 18, 1–37.
Wang, P., Cheng, M., Zhang, Z., 2014. On different photodecomposition behaviors of rhodamine B on laponite and montmorillonite clay under visible light irradiation. J. Saudi Chem. Soc. 18, 308–316.
Zhong, W.W., 2009. Nanomaterials in fluorescence-based biosensing. Anal. Bioanal. Chem. 394, 47–59.
Zhou, C.H., Shen, Z.F., Liu, L.H., Liu, S.M., 2011. Preparation and functionality of clay-containing films. J. Mater. Chem. 21, 15132–15153.
Zwillinger, D., 2003. 7.1.8 geometric probability. In: Zwillinger, D. (Ed.), CRC Standard Mathematical Tables and Formulae, 31st ed. CRC Press, London (p. equation 7.1.46).